Electronic Supporting Information

Field-Induced Slow Magnetic Relaxation In the First Dy(III)-centered 12-Metallacrown-4 Double-Decker Complex

Angeliki A. Athanasopoulou,[1,2] José J. Baldoví [3], Luca M. Carrella,[1] and Eva Rentschler*[1]

1 Institute of Inorganic and Analytical Chemistry, Johannes Gutenberg University Mainz, Duesbergweg 10-14, D-55128 Mainz, Germany

2 Graduate School Materials Science in Mainz, Staudinger Weg 9, D-55128 Mainz, Germany

3 Max Planck Institute for the Structure and Dynamics of Matter, Luruper Chaussee 149, D-22761 Hamburg, Germany

*Corresponding author

Eva Rentschler

Institute of Inorganic and Analytical Chemistry

 Johannes Gutenberg University Mainz

Duesbergweg 10-14

D-55128 Mainz, Germany

Fax: +49 6131 39 23922

Tel: +49 6131 39 25491

E-mail: rentschler@uni-mainz.de

Contents

All manipulations were performed under aerobic conditions using materials (reagent grade) and solvents as received.

C, H and N elemental analyses were carried out on a Foss Heraeus Vario EL at the Institute of Organic Chemistry at the Johannes Gutenberg University Mainz. Infrared absorption spectra were recorded at room temperature in a range of 3,000-400 cm^{-1} on a Thermo Fischer NICOLET Nexus FT/IR-5700 spectrometer equipped with Smart Orbit ATR Diamond cell. UV-Vis absorption measurements were performed between for complexes 1, 2, 3 and 4 in MeCN between 200 and 1000 nm on a JASCO V-570 UV/Vis/NIR spectrophotometer (Fig.S10, ESI) Variable-temperature direct current (dc) magnetic susceptibility measurements were performed on polycrystalline samples with the use of Quantum Design SQUID magnetometer MPMS-7 equipped with a 7 T magnet. The samples were embedded in eicosane to avoid orientation of the crystallites under applied field. Experimental susceptibility data were corrected for the underlying diamagnetism using Pascal's constants.[1] The temperature dependent magnetic contribution of the holder and of the embedding matrix eicosane were experimentally determined and substracted from the measured susceptibility data. Variable temperature susceptibility data were collected in a temperature range of 2-300K under an applied field of 0.1 Tesla, while magnetization data were collected between 2 and 10 K and using magnetic fields up to 7 Tesla. Alternating-current (ac) measurements were performed with an oscillating magnetic field of 3 Oe at frequencies ranging from 1 to 1400 Hz. Field-dependence measurements were performed and they revealed an optimum dc field of 1000 Oe. Using that optimum field further magnetic measurements were performed as described in the text.

Synthesis of reported complex 1

(^{n}Bu$_4$N) {Ga$_8$Dy(OH)$_4$(shi)$_8$}·5MeOH·3H$_2$O (1): To a stirred almost colorless solution of shiH$_3$ (61.00 mg, 0.4 mmol) and piperidine (40 μL, 0.4 mmol) in MeOH, Ga(NO$_3$)$_3$·H$_2$O (109 mg, 0.4 mmol) was added and left for stirring for 5 min. To the resulting clear and colorless solution Dy(O$_2$CMe)$_3$•xH$_2$O (20.00 mg, 0.05 mmol) was added along with ^{n}Bu$_4$NClO$_4$ (52.00 mg, 0.15 mmol) and was stirred for further 1 h. Then, the solution was filtered and the filtrate was left for slow evaporation. Colorless, good diffraction quality crystals of **1** appeared after 2 weeks which were collected by filtration, washed with hexane (3 × 5 mL) and dried in air. Yield: 0.060 g (24.9%) based on the Dy^{III} ion. The air-dried solid was analyzed as **1·5H$_2$O (Ga$_8$Dy$_1$H$_{84}$O$_{34}$C$_{72}$ N$_9$):** C, 36.96; H, 3.62; N, 5.39. Found: C, 36.92; H, 3.53; N, 5.38. Selected ATR data (cm^{-1}): 1603 (s), 1573 (s), 1507 (w), 1442 (w), 1410 (w), 1264 (s), 1247 (w), 939 (s), 863 (s), 683 (w), 660 (w), 448 (w).

Single-crystal X-ray diffraction studies.

X-ray diffraction data for the structure analysis were collected from suitable single crystals on a STOE IPDS 2T[2] equipped with an Oxford cooling system operating at 120(2) K (1), respectively. Graphite-monochromated Mo-Kα radiation (λ = 0.71073 Å) from long-fine focus sealed X-ray tube was used throughout. Data indexing, reduction, integration and absorption correction were done with STOE X-AREA and STOE X-RED[2]. Structures were solved with SHELXT[3] and refined by full-matrix least-squares on F-squared using SHELXL[4], interfaced through OLEX2-1.2[5]. All non-hydrogen atoms were refined with anisotropic displacement parameters, while hydrogen atoms have been placed on idealized position using a riding model. For the solvent water molecules the hydrogen atoms cannot be located properly and were omitted. The tetrabutylammonium counter ion is highly disordered over several positions. Only the two main, symmetry related, positions were taken into account. CCDC 1903450 contains the supplementary crystallographic data for the structure reported in this paper. These data can be obtained free of charge via www.ccdc.cam.ac.uk/conts/retrieving.html (or from the Cambridge Crystallographic Data Centre, 12 Union Road, Cambridge CB21EZ, UK; fax: (+44)1223-336-033; or deposit@ccdc.cam.ac.uk).

Table S1. Crystallographic data for complex **1**.

Complex	**1**•5MeOH•3H$_2$O
Empirical formula	C$_{77}$H$_{92}$Ga$_8$DyN$_9$O$_{36}$
Formula weight	2439.85
Temperature/K	120 (2)
Crystal system	monoclinic
Space group	P 2/*c*
a/Å	13.6911 (4)
b/Å	18.1247(5)
c/Å	19.8116(5)
α/°	90
β/°	90.093 (2)
γ/°	90
Volume/Å^3	4916.2(2)
Z	2
ρ$_{calc}$g/cm^3	1.648
μ/mm^{-1}	2.990
F(000)	2438.0
Crystal size/mm^3	0.38 × 0.263 × 0.09
Radiation	MoK\α (λ = 0.71073)
2Θ range for data collection/°	5.072 to 53.772
Index ranges	-17 ≤ h ≤ 17 -23 ≤ k ≤ 22 -25≤ l ≤ 21
Reflections collected	24260
Independent reflections	R$_{int}$ = 0.0375 R$_{sigma}$ = 0.0341
Data/restraints/ parameters	10530 / 68 / 679
Goodness-of-fit on F^2	1.165
Final R^{a,b} indexes [I>=2σ (I)]	R$_1$ = 0.0973 wR$_2$ = 0.2554
Final R ^{a,b} indexes [all data]	R$_1$ = 0.1082 wR$_2$ = 0.2648
Largest diff. peak /hole / e Å^{-3}	4.55/ -1.87

[a]R$_1$ = Σ(||F$_o$| − |F$_c$||)/Σ|F$_o$|. [b]wR$_2$ = [Σ[w(F$_o^2$ - F$_c^2$)^2]/Σ[w(F$_o^2$)^2]]$^{1/2}$, w = 1/[σ^2(F$_o^2$) + (ap)^2 + bp], where p = [max(F$_o^2$, 0) + 2F$_c^2$]/3.

Table S2. Selected Bond Lengths for complex **1.**

Atom	Atom	Length/Å
Dy1	O3	2.329(6)
Dy1	O6	2.342(7)
Dy1	O9	2.308(6)
Dy1	O12	2.312(6)
Ga1	O1	1.869(6)
Ga1	O11	1.915(7)
Ga1	O12	1.955(6)
Ga1	O13	1.865(7)
Ga1	N1	1.978(8)
Ga2	O2	1.923(7)
Ga2	O3	1.957(7)
Ga2	O4	1.870(7)
Ga2	O13[1]	1.865(7)
Ga2	N2	1.985(8)
Ga3	O5	1.956(8)
Ga3	O6	1.942(7)
Ga3	O7	1.840(8)
Ga3	O14[1]	1.866(8)
Ga3	N3	1.977(9)
Ga4	O8	1.913(8)
Ga4	O9	1.950(7)
Ga4	O10	1.870(7)
Ga4	O14	1.885(8)
Ga4	N4	1.959(8)
O1	C1	1.356(11)
O2	C7	1.295(12)
O3	N1	1.396(9)
O6	N2	1.424(10)
O9	N3	1.413(11)
O12	N4	1.422 (9)

[1]1-X,+Y,3/2-Z

Table S3 Selected Bond Angles for **1.**

Atom	Atom	Atom	Angle/°
O3^1	Dy1	O3	80.7(3)
O3	Dy1	O6^1	138.3(2)
O3	Dy1	O6	68.7(2)
O6	Dy1	O6^1	150.9(3)
O9	Dy1	O3	107.9(2)
O9	Dy1	O3^1	150.8(2)
O9^1	Dy1	O6	88.5(2)
O9	Dy1	O6	68.7(2)
O9	Dy1	O9^1	78.5(3)
O9^1	Dy1	O12	135.8(2)
O9	Dy1	O12	71.7(2)
O12	Dy1	O3	71.4(2)
O12^1	Dy1	O3	85.7(2)
O12	Dy1	O6^1	78.5(2)
O12	Dy1	O6	109.3(2)
O12^1	Dy1	O12	149.9(3)
O1	Ga1	O11	87.9(3)
O1	Ga1	O12	159.5(3)
O1	Ga1	N1	92.8(3)
O11	Ga1	O12	80.0(3)
O11	Ga1	N1	144.0(3)
O12	Ga1	N1	87.6(3)
O13	Ga1	O1	102.0(3)
O13	Ga1	O11	105.4(3)
O13	Ga1	O12	97.2(2)
O13	Ga1	N1	109.5(3)
O2	Ga2	O3	80.6(3)
O2	Ga2	N2	145.5(3)
N4	O12	Ga1	113.3(5)

^{1}1-X,+Y,3/2-Z
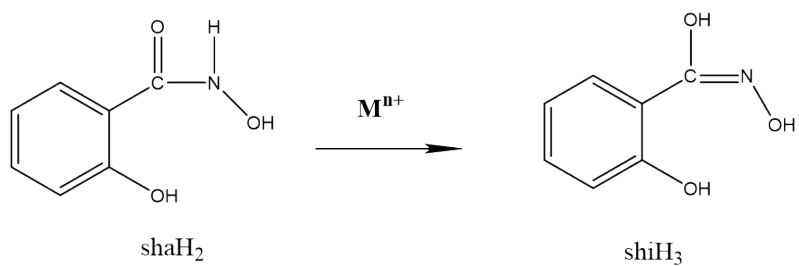
Scheme 1. Illustrative representation and abbreviation of the metal assisted 2-amide-iminol tautomerism of organic molecules discussed in the text.[6,7]
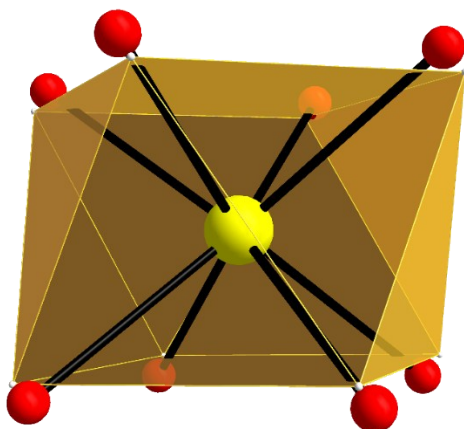

Figure S1. Square antiprismatic geometry of central lanthanide in complex **1**. The points connected by the lighter lines define the vertices of the ideal polyhedron. Color scheme: Ln, yellow; O, red.

Table S4. Shape measurements of the 8-coordinate lanthanide coordination polyhedra. The bold numbers indicate the closest polyhedron according to SHAPE calculations.[8]

Polyhedron[c]	Dy1
OP-8	34.44
HPY-8	22.71
HBPY-8	13.83
CU-8	6.56
SAPR-8	**1.18**
TDD-8	2.26
JGBF-8	16.57
JETBPY-8	28.70
JBTPR-8	3.85
BTPR-8	3.29
JSD-8	6.16
TT-8	7.45
ETBPY-8	25.63

[c] Abbreviations: OP-8, octagon; HPY-8, heptagonal pyramid; HBPY-8, hexagonal bipyramid; CU-8, cube; SAPR-8, square antiprism; TDD-8, triangular dodecahedron; JGBF-8, Johnson gyrobifastigium; JETBPY-8, Johnson elongated triangular bipyramid; JBTPR-8, Johnson biaugmented trigonal prism; BTPR-8, biaugmented trigonal prism; JSD-8, Johnson snub diphenoid; TT-8, triakis tetrahedron; ETBPY-8, elongated trigonal bipyramid.
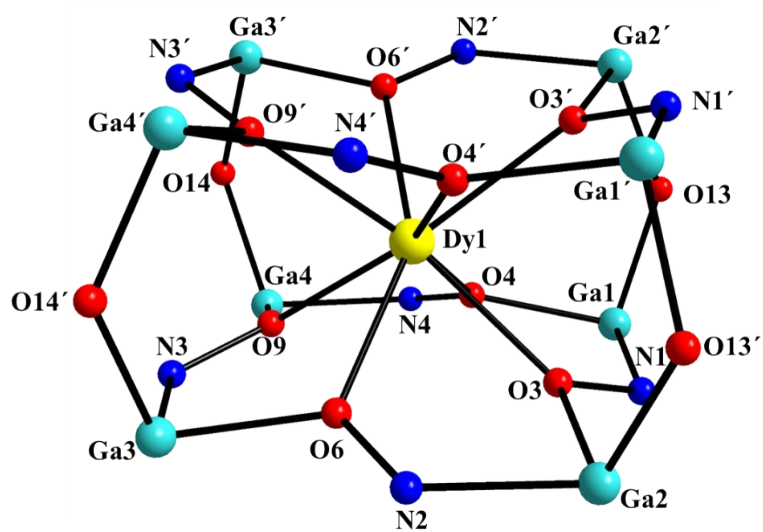
Figure S2. Labelled schematic representation of the core {Ga$^{III}_8$Dy^{III}(μ-OH)$_4$(μ-NO)$_8$}$^{15+}$ of **1**. Color scheme: Ga^{III}, aqua; Dy^{III}, yellow; N, blue; O, red; C, black. H atoms are omitted for clarity.
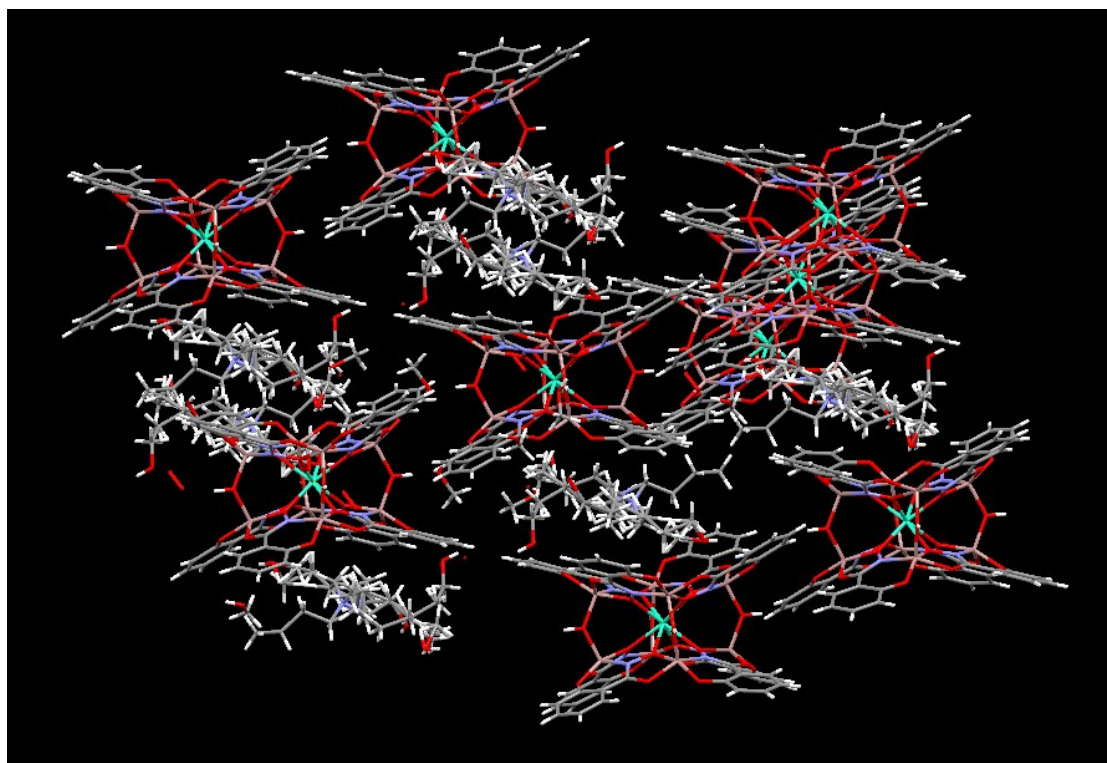

Figure S3. Schematic representation of crystal packing of the molecules of compound **1**.
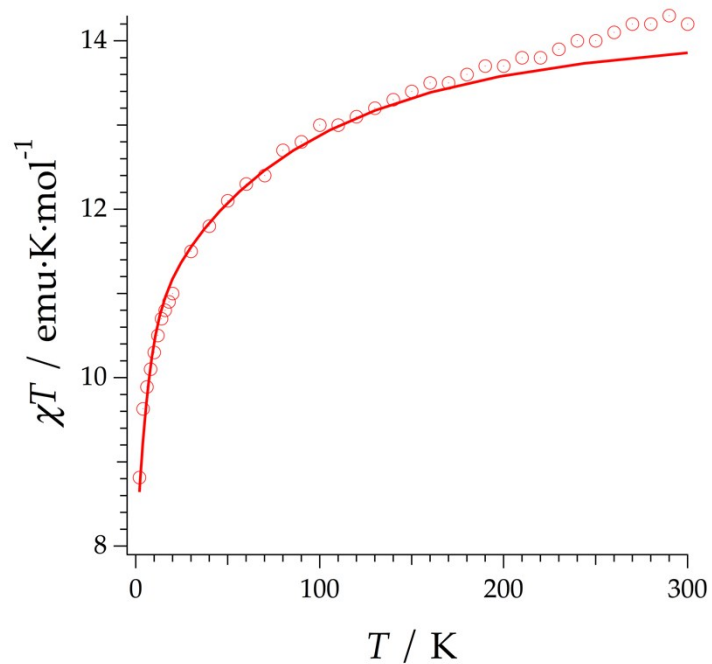
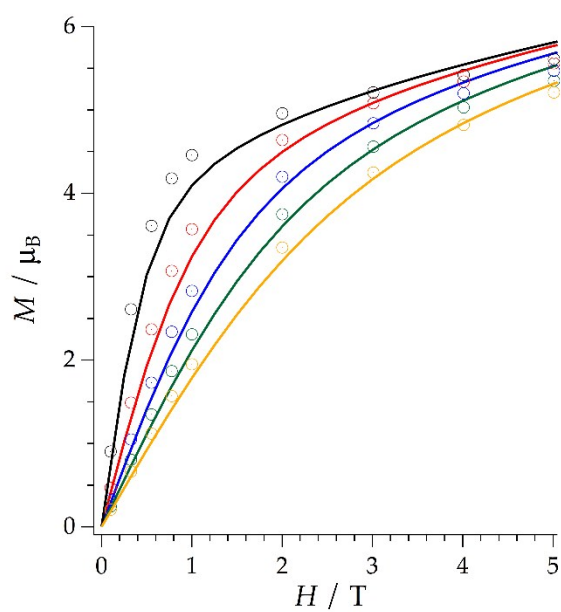**Figure S4.** Experimental (symbols), fitted (solid line) thermal dependence of the magnetic susceptibility of **1** from 2 to 300 K measured at 1000 Oe.

Figure S5. M vs H plots for complex **1** at various temperatures. The figure shows experimental (symbols) and predicted (solid line) magnetization versus magnetic field at 2 (black), 4 (red), 6 (blue), 8 (green) and 10 K (orange).
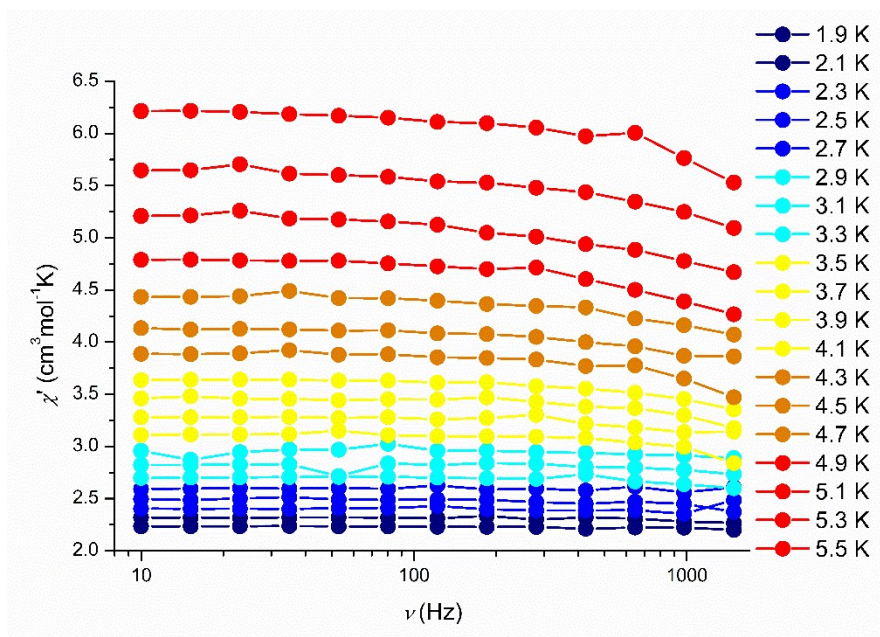
Figure S6. Frequency dependent in-phase susceptibility plot of for compound **1** (1.9 to 5.5 K) at 0 Oe. Solid lines represent guidelines for the eyes.
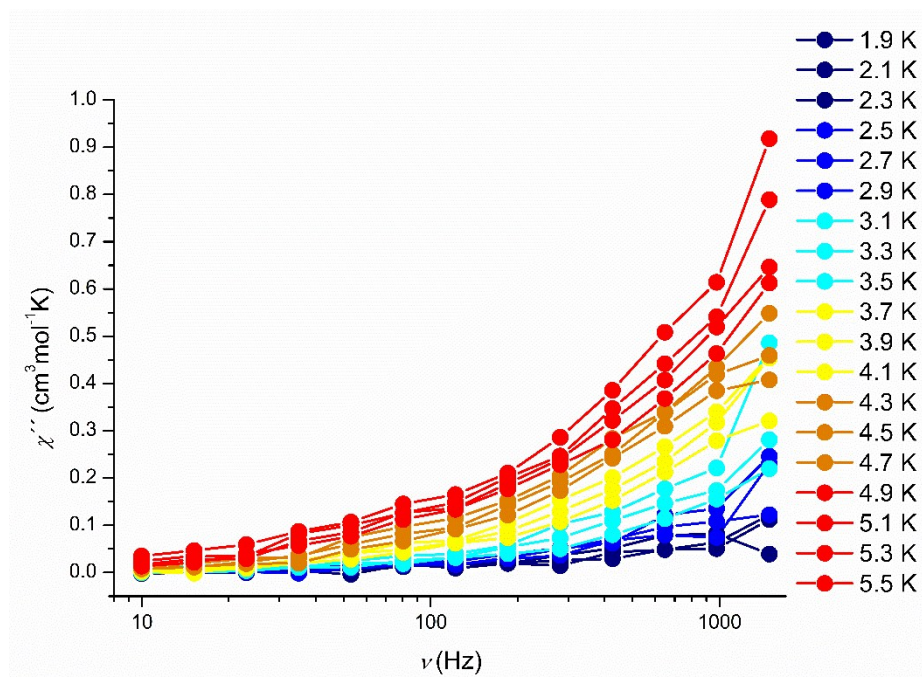

Figure S7. Frequency dependent out-of-phase susceptibility plot of for compound **1** (1.9 to 5.5 K) at 0 Oe. Solid lines represent guidelines for the eyes.
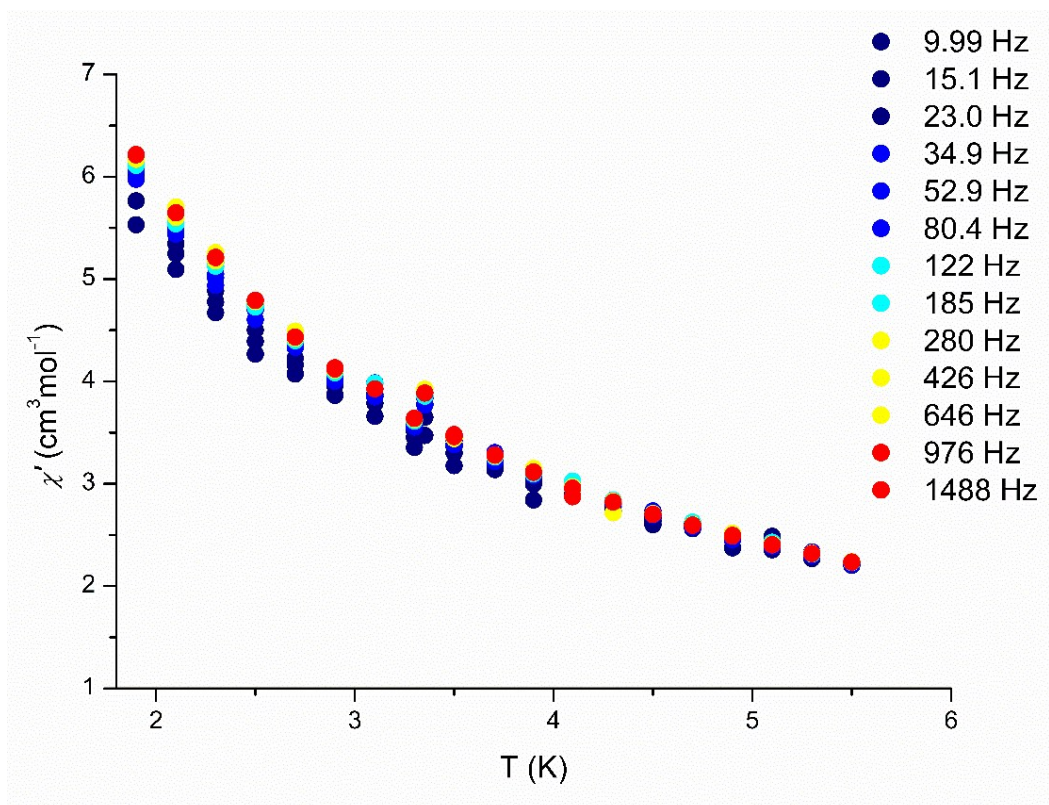
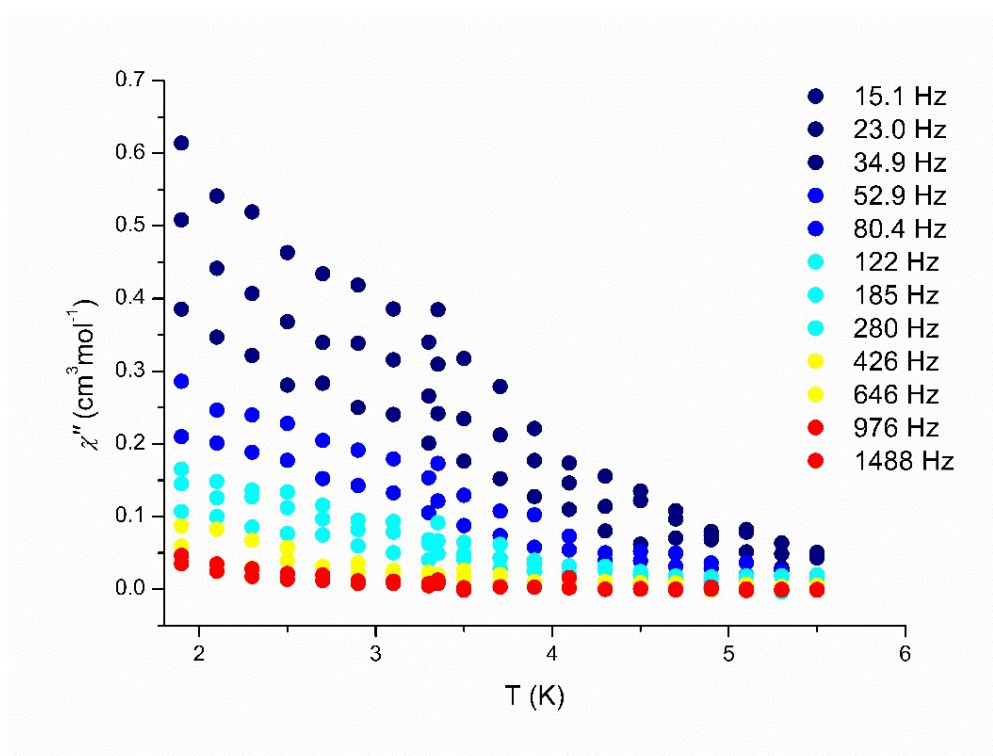**Figure S8.** Temperature dependent in-phase susceptibility plot of for compound **1** (1.9 to 5.5 K) at 0 Oe.

Figure S9. Temperature dependent in-phase susceptibility plot of for compound **1** (1.9 to 5.5 K) at 0 Oe.
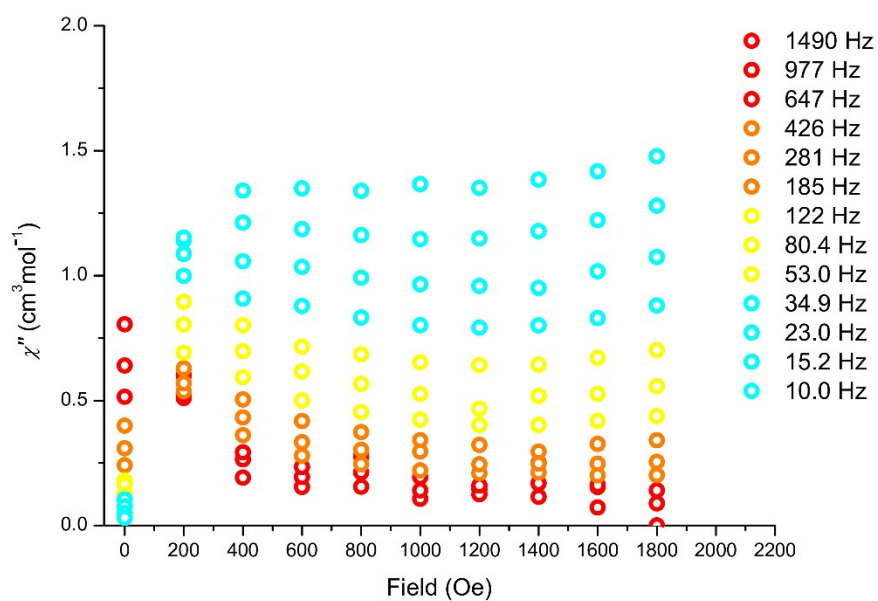
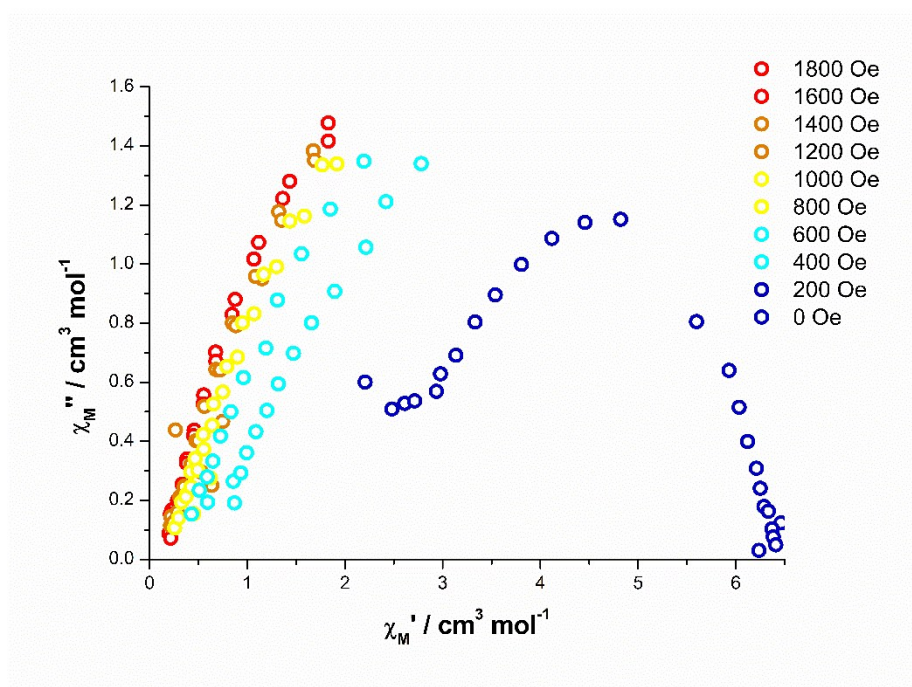**Figure S10**. Field scan measurements for compound **1** at 2 K.

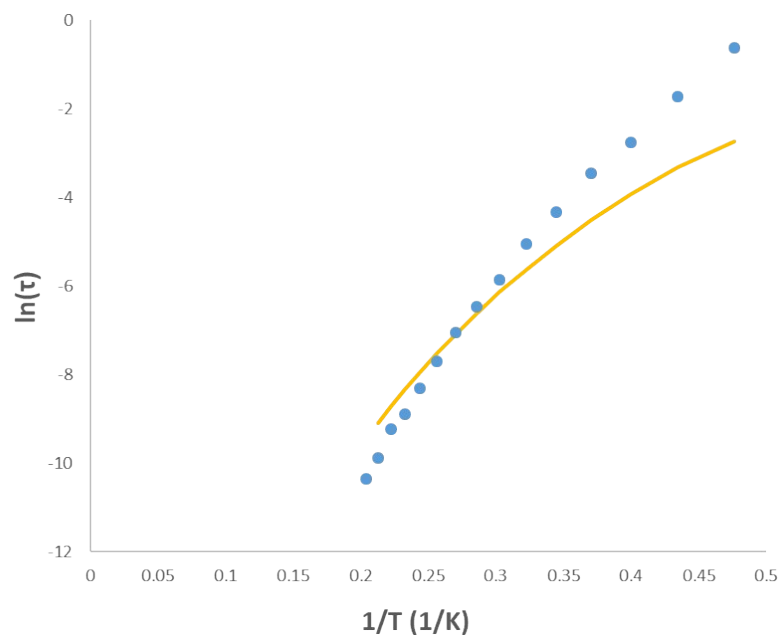**Figure S11**. Field-dependent Cole-Cole plots for compound **1**.

Figure S12. Arrhenius plot showing the magnetization relaxation of **1** under an applied field of 1000 Oe. The yellow line represents fitting of the data using solely the Raman relaxation process.

Fitting of the data, using exclusively the Raman process and by letting the n parameter free, gave n = 8.78(4) and C = 0.00769(5) $s^{-1}K^{-8.78}$. The fitting performed could not yield satisfactory parameters, however since the Raman contribution for our compound is evidently strong, we performed the fitting with the best obtained attempt shown at the Figure S12. Obviously, the Orbach contibution dominates at the high temperature regime, as can be realised by comparing the figures possesing both the fitting procedures. Fitting of the data using the Orcbach and Raman processes can be found in the main text at Figure 5.

UV-Vis Absorption Spectroscopy

The ligand (shiH$_3$) has three bands at 220 nm, 248 nm and 263 nm, which appear to be also present at the complex. These ligand-centered transitions, that can be assigned to excitations within the delocalized π-system of the coordinated hydroxamic acid, are observed at 238, 264 and 307 nm for **1**.
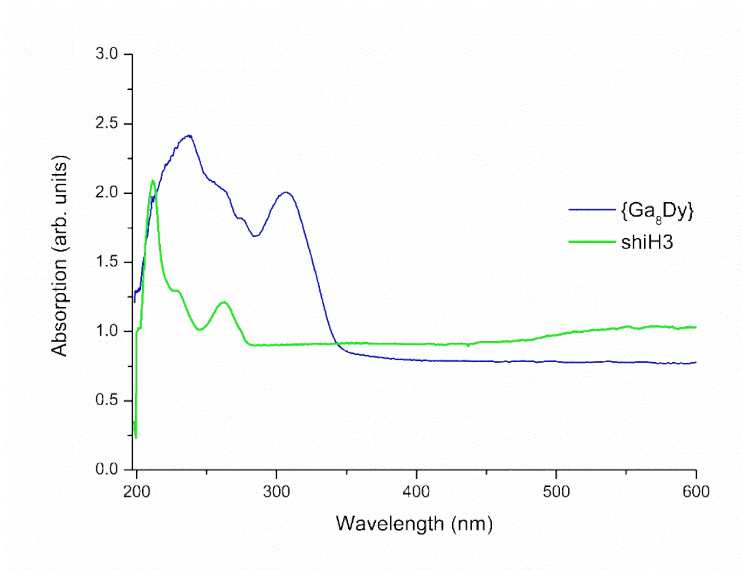

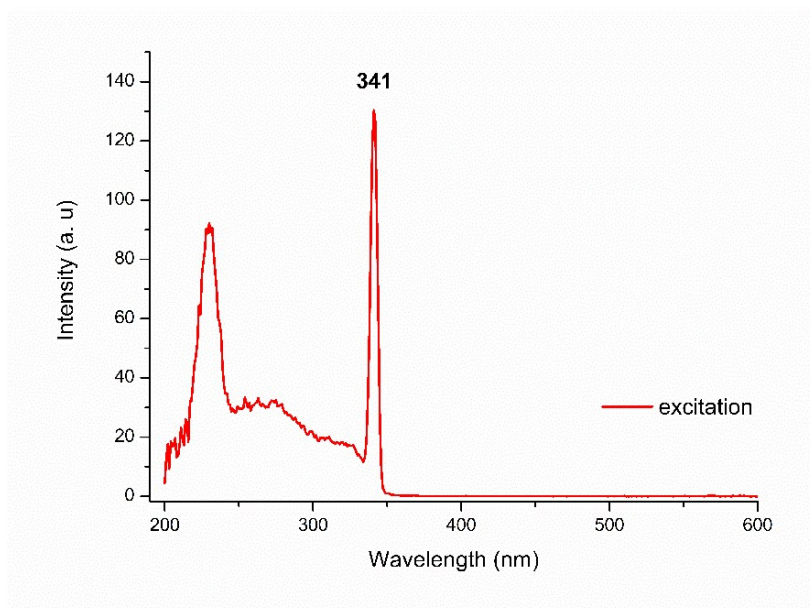**Figure S13**. UV-vis studies for complex **1** and shiH$_3$ in MeCN.

Figure S14. Room temperature excitation spectra for **1** in MeCN.
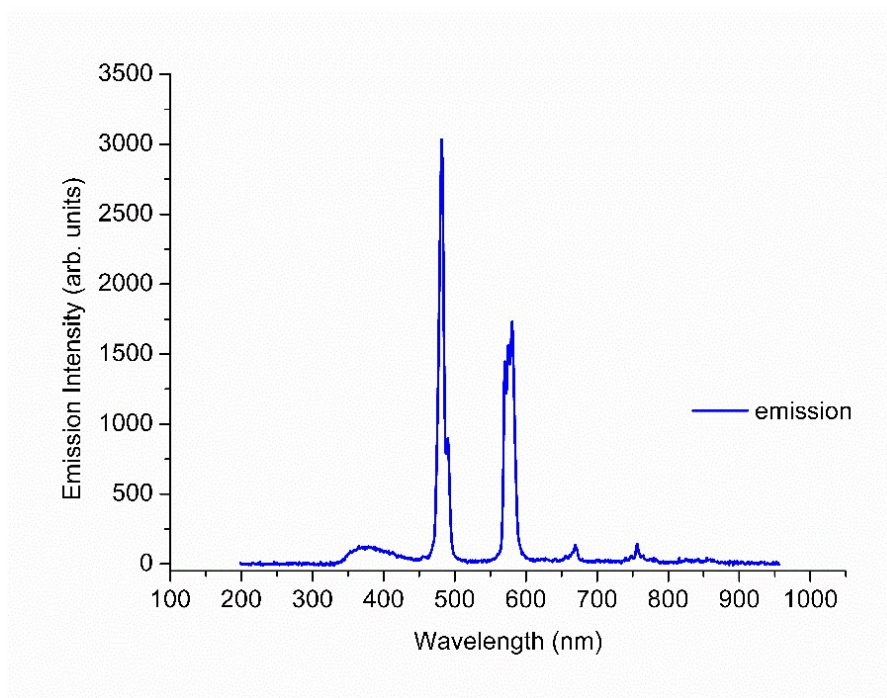
Figure S15. Room temperature emission spectra for **1** in MeCN. The excitation wavelength was 340 nm.
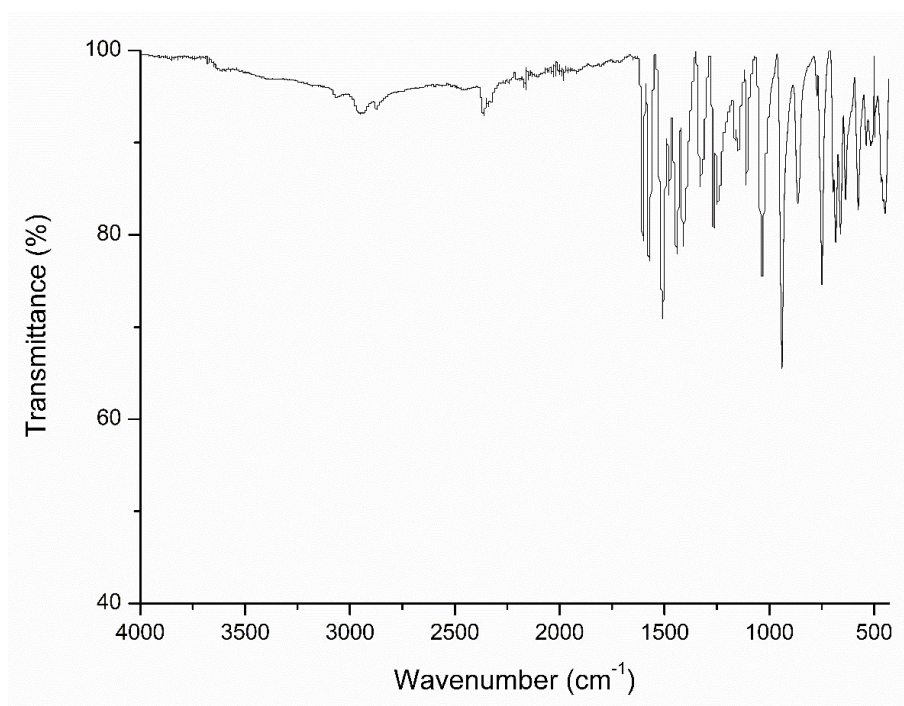

Figure S16. IR spectrum for complex **1**.

SIMPRE software

The static magnetic properties have been rationalized using the SIMPRE computational package.[9,10] The experimental atomic coordinates and magnetic susceptibility data have been introduced as an input; the two fitting parameters (D_r and Z_i) of the Radial Effective Charge (REC) model have been scanned.[11] A detailed explanation is provided in the Supporting Information.

Radial Effective Charge (REC) model

Theoretical approach

Our calculations start with the crystallographic atomic coordinates of the first coordination sphere. These are introduced as an input in the *simpre.dat* file of the portable *fortran77* software code SIMPRE.[9,12] This code parameterizes the electric field effect produced by the surrounding ligands, acting over the central ion, by using the following Crystal Field Hamiltonian expressed in terms of the Extended Stevens Operators (ESOs)[13–15]:

$$\hat{H}_{cf}(J) = \sum_{k=2,4,6} \sum_{q=-k}^{k} B_k^q O_k^q = \sum_{k=2,4,6} \sum_{q=-k}^{k} a_k (1-\sigma_k) A_k^q \langle r^k \rangle O_k^q$$

where k is the order (also called rank or degree) and q is the operator range, that varies between k and $-k$, of the Stevens operator equivalents O_k^q as defined by Ryabov in terms of the angular momentum operators $J_\pm$ and J_z,[16] where the components $O_k^q(c)$ and $O_k^q(s)$ correspond to the ESOs with q $\geq$ 0 and q < 0 respectively.[16] Note that all the Stevens CF parameters B_k^q are real, whereas the matrix elements of O_k^q (q < O) are imaginary. a_k are the α, β and γ Stevens coefficients[17] for k = 2, 4, 6, respectively, which are tabulated and depend on the number of f electrons. σ_k are the Sternheimer shielding parameters of the 4f electronic shell, and <r^k> are the expectation values of the radius.[18]

In SIMPRE, the A_k^q CF parameters are determined by the following relations:

$$A_k^0 = \frac{4\pi}{2k+1} \sum_{i=1}^{N} \frac{Z_i e^2}{R_i^{k+1}} Z_{k0}(\theta_i, \varphi_i) p_{kq} \tag{2a}$$

$$A_k^q = \frac{4\pi}{2k+1} \sum_{i=1}^{N} \frac{Z_i e^2}{R_i^{k+1}} Z_{kq}^c(\theta_i, \varphi_i) p_{kq} \quad (q>0) \tag{2b}$$

$$A_k^q = \frac{4\pi}{2k+1} \sum_{i=1}^{N} \frac{Z_i e^2}{R_i^{k+1}} Z_{k|q|}^s(\theta_i, \varphi_i) p_{k|q|}$$

where R_i, θ_i and φ_i are the effective polar coordinates of the point charges, and Z_i is the effective point charge, associated to the *i*-th donor atom with the lanthanoid at the origin, *N* is the number of ligands; *e* is the electron charge, p_{kq} are the prefactors of the spherical harmonics and Z_{kq} are the tesseral harmonics expressed in terms of the polar coordinates for the i-th donor atom.

In the REC model[11] the ligand is modeled through an effective point charge situated between the lanthanoid and the coordinated atom at a distance R_i from the magnetic centre, which is smaller than the real metal-ligand distance (r_i). To account for the effect of covalent electron sharing, a radial displacement vector (D_r) is defined, in which the polar coordinate *r* of each coordinated atom is collectively varied, $R_i = r_i\text{-}D_r$, and at the same time the charge value (Z_i) is scanned in order to achieve a minimum deviation between calculated and experimental data, whereas θ_i and φ_i remain constant. In the fitting procedures, we define the relative error *E* as:

$$E = \frac{1}{n}\sum_{i=1}^{n}\frac{\left[\chi_{theo,i} - \chi_{\exp,i}\right]^2}{\left[\chi_{\exp,i}\right]^2} \qquad (3)$$

where χ_{exp} and χ_{theo} are experimental and theoretical magnetic susceptibility, respectively, and *n* is the number of points.

Table S5. Ground multiplet energy level scheme (cm^{-1}) and main $|M_J\rangle$ contributions (more than 10%) to the wave function calculated for complex **1**.

E (cm^{-1})	Wave function amplitudes
0	79% $|\pm11/2\rangle$
15	81% $|\pm13/2\rangle$
148	61% $|\pm9/2\rangle$ + 19% $|\pm7/2\rangle$ + 10% $|\pm11/2\rangle$
228	35% $|\pm7/2\rangle$ + 23% $|\pm5/2\rangle$ + 13% $|\pm1/2\rangle$ + 11% $|\pm9/2\rangle$
270	22% $|\pm3/2\rangle$ + 19% $|\pm5/2\rangle$ + 16% $|\pm1/2\rangle$ + 13% $|\mp3/2\rangle$ + 13% $|\mp7/2\rangle$
389	45% $|\pm1/2\rangle$ + 14% $|\pm3/2\rangle$
441	37% $|\pm5/2\rangle$ + 33% $|\mp3/2\rangle$ + 17% $|\pm7/2\rangle$
549	93% $|\pm15/2\rangle$

Table S6. Crystal-field parameters in cm^{-1} (Stevens notation) obtained for **1**.

k	q	$A_k^q\langle r^k\rangle$	B_k^q
2	0	30.61	-0.19434
2	1	51.67	-0.32805
2	-1	-228.01	1.44770
2	2	51.37	-0.32613
2	-2	24.52	-0.15566
4	0	-222.68	0.01318
4	1	-127.28	0.00754
4	-1	561.12	-0.03322
4	2	126.99	-0.00752
4	-2	60.68	-0.00359
4	3	341.91	-0.02024
4	-3	-433.66	0.02567
4	4	151.81	-0.00899
4	-4	187.62	-0.01111
6	0	76.76	0.00008
6	1	43.46	0.00004
6	-1	-191.32	-0.00020
6	2	-141.00	-0.00015
6	-2	-67.28	-0.00007

References

[1]   G. A. Bain, J. F. Berry, *Journal of Chemical Education* **2008**, *85*, 532.

[2]   Stoe & Cie X-AREA 2002, Stoe &Cie X-RED 2002, Stoe & Cie, Darmastadt, Germany.

[3]   G. M. Sheldrick, *Acta Crystallographica Section A Foundations and Advances* **2015**, *71*, 3–8.

[4]   G. M. Sheldrick, *Acta Crystallographica Section C Structural Chemistry* **2015**, *71*, 3–8.

[5]   O. V. Dolomanov, L. J. Bourhis, R. J. Gildea, J. A. K. Howard, H. Puschmann, *Journal of Applied Crystallography* **2009**, *42*, 339–341.

[6]   C. Y. Chow, E. R. Trivedi, V. Pecoraro, C. M. Zaleski, *Comments on Inorganic Chemistry* **2015**, *35*, 214–253.

[7]   G. Mezei, C. M. Zaleski, V. L. Pecoraro, *Chemical Reviews* **2007**, *107*, 4933–5003.

[8]   S. Alvarez, P. Alemany, D. Casanova, J. Cirera, M. Llunell, D. Avnir, *Coordination Chemistry Reviews* **2005**, *249*, 1693–1708.

[9]   J. J. Baldoví, S. Cardona-Serra, J. M. Clemente-Juan, E. Coronado, A. Gaita-Ariño, A. Palii, *Journal of Computational Chemistry* **2013**, *34*, 1961–1967.

[10] J. J. Baldoví, J. M. Clemente-Juan, E. Coronado, A. Gaita-Ariño, A. Palii, *Journal of Computational Chemistry* **2014**, *35*, 1930–1934.

[11] J. J. Baldoví, J. J. Borrás-Almenar, J. M. Clemente-Juan, E. Coronado, A. Gaita-Ariño, *Dalton Transactions* **2012**, *41*, 13705.

[12] J. J. Baldoví, J. M. Clemente-Juan, E. Coronado, A. Gaita-Ariño, A. Palii, *Journal of Computational Chemistry* **2014**, *35*, 1930–1934.

[13] C Rudowicz, *J. Phys. C: Solid State Phys* **1985**, *18*, 3837.

[14] C. Y. C. C. Rudowicz, *J. Phys. Condes. Matter* **2004**, *16*, 5825.

[15] C. Rudowicz, *J. Phys. C: Solid State Phys.* **n.d.**, *18*, 1415.

[16] I. D. Ryabov, *Journal of Magnetic Resonance* **1999**, *140*, 141–145.

[17] K W H Stevens, *Proc. Phys. Soc. A* **1952**, *65*, 209.

[18] M. K. S. Edvardsson, *Journal of Alloys and Compounds* **1998**, *275*, 233.